Materials Research. 2021; 24(suppl. 1): e20210029
DOI: https://doi.org/10.1590/1980-5373-MR-2021-0029

The Plasmonic Effect of Gold Nanorods on Charged Molecules: SERRS and SEF effects

Tatiana Aparecida Oliveira[a], *Rafael Jesus Gonçalves Rubira*[a], *Cibely da Silva Martin*[a]*, *Anerise de Barros*[b], *Italo Odone Mazali*[b], *Carlos José Leopoldo Constantino*[a]

[a]*Universidade Estadual Paulista (UNESP), Faculdade de Ciências e Tecnologia, Departamento de Física, 19060-900, Presidente Prudente, SP, Brasil.*
[b]*Universidade Estadual de Campinas (UNICAMP), Instituto de Química, Laboratório de Materiais Funcionais, 13083-970, Campinas, SP, Brasil.*

Received: January 12, 2021; Revised: May 08, 2021; Accepted: June 16, 2021

Target molecules adsorbed onto metallic nanoparticles can have their Raman and/or fluorescence signals enhanced, leading to the called surface-enhanced [resonance] Raman scattering (SE[R]RS) or surface-enhanced fluorescence (SEF). Here we have applied Au nanorods (AuNRs) coated with a surfactant bilayer leading to a positive surface charge to investigate the role played by these AuNRs in colloidal suspension on SERRS and SEF effects of charged molecules. In the case of the anionic nickel (II) tetrasulfonated phthalocyanine (NiTsPc), besides achieving SERRS with an enhancement factor (EF) of ca. 10^5, the AuNRs allowed the analytical application of the SERRS effect for the NiTsPc between $8.3x10^{-6}$ and $4.0x10^{-5}$ mol L^{-1}. The limit of detection of $4.8x10^{-7}$ mol L^{-1} (at 752 cm^{-1}) and $1.3x10^{-6}$ mol L^{-1} (at 1338 cm^{-1}) was found. In the case of the cationic methylene blue, the SEF effect was achieved reaching an EF of ca. 10. Besides, fundamental discussions are carried out considering the results presented here.

Keywords: gold nanorods, SERRS, SEF, charge effect.

1. Introduction

The inelastic light scattering represented by the Raman scattering spectroscopy has a low cross-section (ca. 10^{-29} cm^2/molecule), which is a limitation of the technique when applied in the analysis of ultrathin films (monolayers or a few nanometers of thickness) or highly diluted solutions (<10^{-8} mol/L), for instance[1,2]. However, the adsorption of target molecules onto rough metallic surfaces, or nanoparticle surface, can promote an enhancement of the Raman signal, leading to the called surface-enhanced Raman scattering (SERS)[3,4]. Therefore, the SERS technique can provide not only the molecule fingerprint through its vibrational spectrum (selectivity) but also allow the detection of target molecules at pretty low concentrations (sensitivity)[5,6]. Besides, when the wavelength of the excitation laser line is within the electronic absorption band of the target molecule, the resonance phenomenon is involved, resulting in the resonance Raman scattering (RRS), or surface-enhanced resonance Raman scattering (SERRS) when in the presence of nanoparticles[7,8].

Briefly, considering the Raman signal from a target molecule is given by the induced dipole $\vec{p} = \tilde{\alpha}.\vec{E}$ ($\tilde{\alpha}$: target molecule polarizability; $\vec{E}$: incident electromagnetic field), the Raman signal enhancement (SERS) has its origin in the enhancement of the electromagnetic field surrounding the nanoparticles, named Local Field: $\vec{E_L} \rightarrow \vec{p}_{SERS} = \tilde{\alpha}.\vec{E_L}$, which is much larger than the incident electromagnetic field ($\vec{E}$) and supported by the localized surface plasmon resonances (LSPR). This process is named "electromagnetic mechanism" and can lead to enhancement factors (EF) of the Raman signal up to 10^6. Usually, Cu, Ag, and Au are applied to enhance the electromagnetic field when the excitation is achieved by laser lines in the visible range. It is important to mention that not only the Raman scattering (or RRS) but also other optical processes such as absorption (SEIRA: surface-enhanced infrared absorption) and emission (SEF: surface-enhanced fluorescence, also known as MEF: metal-enhanced fluorescence) can be benefited by the "electromagnetic mechanism"[2]. Complementary, the formation of a metal-target molecule complex can also provide an enhancement of the Raman signal by changes on the target molecule polarizability: $\tilde{\alpha} \rightarrow \tilde{\alpha}_{complex} \rightarrow \vec{p}_{SERS} = \tilde{\alpha}_{complex}.\vec{E_L}$. The latter is named "chemical (or electronic)" effect and leads to EF up to 10^2 (or 10^3 under resonant conditions[9]).

Thus, either SERS or SERRS are potential tools for analytical application due to their high selectivity and sensibility[4]. However, the EF of the Raman signal leading to SERS or SERRS depends on parameters such as: dielectric functions of the metal and the medium surrounding the nanoparticles at the wavelength of the excitation laser line, adsorption mechanism of the target molecule onto the metal surface (distance dependence), and size, shape, and distribution (aggregation) of the metallic nanoparticles[2]. The latter, which is directly related to the SERS platform (substrate) homogeneity, is not a straightforward parameter to be controlled, especially when nanoparticle aggregation

*e-mail: cssmartin@gmail.com

is involved. It is quite difficult to obtain reproducible homogeneous SERS platforms that would lead to reproducible SERS signals (in terms of EF). This reproducibility against SERS homogeneous platforms remains a challenge, still nowadays, for the application of SERS or SERRS as routine analytical tools. For instance[2], molecules adsorbed within interstitial regions among nanoparticles can reach EF up to 10^{10}. These regions are called hot spots and allow single molecule detection using SERS[10,11] or SERRS[12].

Based on this, the development of appropriated SERS or SERRS platforms plays a key role to obtain reproducible EF, besides selectivity, and sensibility. Among SERS or SERRS platforms, colloidal dispersions (nanoparticle) have been widely applied to SERS analysis in many research areas such as nanobiotechnology[13-15], sensing detection[16-19], disease diagnostics (in vivo system)[6,20-22], and drug delivery[23,24]. The main advantage of the colloidal system is the possibility of modulating the nanoparticle plasmonic properties through shape, size[25], and surface modifications (coating layer and/or functionalization)[26,27]. The latter can change the surface charge, influencing the chemisorption or physisorption of the target molecules onto the nanoparticle surface. In general, metallic nanoparticles show negative charge surfaces, which can difficult the adsorption of anionic molecules[28], but can favor the adsorption of cationic ones through electrostatic interactions[29]. The gold nanorods (AuNRs) coated with a CTAB bilayer have received an increasing interest in the SERS application due to the presence of transverse and longitudinal plasmon resonance and the positive surface charge (provide by CTAB bilayer)[30]. Li et al.[30] described a modification of AuNR surface through the addition of graphene oxide (GO), whose results indicated that the presence of CTAB bilayer around the AuNRs provides a reduction of the structural defects of GO and an improvement on SERS efficiency[30].

The development of nanoparticles for SERS or SERRS applications requests the characterization of the nanoparticle (surface) properties[31]. The nanoparticle surface characterization can involve the use of target molecules with strong Raman signal, such as metallic tetrasulfonated phthalocyanine (MTsPc)[32,33] and dyes[34]. Xu et al.[35] applied SERS and AuNR substrate to detect MB and malachite green (MG) dyes in fish tissues at concentrations of 0.5 and 0.1 ng mL^{-1}, respectively. Chen et al.[36] used MB as a test molecule to enhance the SERS signal of the substrate of molybdenum oxide nanoparticle with graphene in the detection of pollutants. In Lokesh et al.[37] Au and Ag nanoparticles were stabilized using phthalocyanine macrocycle containing functional amine groups, which interact with the nanoparticle, providing better SERS intensity for sensing applications[37].

In this work, we evaluated the plasmonic effect of AuNRs (coated with a CTAB bilayer) on SERRS and SEF effects of charged molecules. For this proposal, we used the anionic NiTsPc and the cationic MB as target molecules. Previously, besides the transmission electron microscopy (TEM) images of the AuNRs, their zeta potential, diffusion motion (rotational and translational - DLS), and UV-vis extinction spectra were monitored in the presence and absence of the target molecules. The SERRS effect was achieved for NiTsPc and the SEF one for MB. In the case of NiTsPc, the SERRS signal was also applied as an analytical tool, which was possible due to the reproducibility of the synthesized AuNRs in terms of size and shape, and their chemical stability in terms of aggregation when in the presence of the target molecules.

2. Materials and Methods

2.1. Reagents

Tetrachloroauric(III) acid ($HAuCl_4.3H_2O$, 393.83 g/mol, Sigma-Aldrich), sodium tetrahydridoborate ($NaBH_4$, 37.83 g/mol, Sigma-Aldrich), hexadecyltrimethylammonium bromide (CTAB, 364.45 g/mol, Sigma-Aldrich), silver nitrate ($AgNO_3$, 169.88 g/mol, Sigma-Aldrich), sodium hydroxide (NaOH, 40 g/mol, Synth), and hydrogen peroxide (H_2O_2, 30%, Synth) were used in the AuNR synthesis. Nickel (II) tetrasulfonated phthalocyanine (NiTsPc, 979.43 g/mol, Sigma-Aldrich) and methylene blue (MB, 319.85 g/mol, Sigma-Aldrich) were used as target molecules (Figure 1). All chemicals were acquired with a purity higher than 99%. All solutions were prepared using ultrapure water with 18.2 MΩ resistivity, acquired from a Milli-Q system (model Simplicity).

2.2. AuNR colloidal synthesis

AuNRs were synthesized by seed-mediated method[38]. Briefly, the synthesis is based on the mixture of two solutions: (i) seed and (ii) growth solutions, as follow:

(i) **seed solution**: it was prepared by adding 24 μL of $NaBH_4$ (0.1 mol L^{-1}) solution (an ice-cold freshly prepared) into a solution composed by 40.5 μL of $HAuCl_4.3H_2O$ (25.4 mmol L^{-1}) and 4.0 mL of CTAB (0.1 mol L^{-1}). The seed solution was stirred for 2 minutes and kept at 28° C for 2 hours.

(ii) **growth solution**: it was prepared by the sequential addition of 25.0 μL of $AgNO_3$ (0.1 mol L^{-1}), 1030.0 μL of $HAuCl_4.3H_2O$ (24.28 mmol L^{-1}), 167.0 μL of NaOH (1.0 mol L^{-1}), and 28.0 μL H_2O_2 (30%) into a 40.0 mL of CTAB (0.1 mol L^{-1}) aqueous solution. The growth solution was stirred for 2 minutes at 28 °C.

Then, 150.0 μL seed solution was added into the total volume of the growth solution. The mixture was stirred for 30 seconds and kept in a bath at 28 °C for 2 hours. The final suspension was centrifuged and resuspended in ultrapure water to complete a final volume of 10 mL. The AuNR colloid was diluted to a concentration of $27x10^{-3}$ mol L^{-1} and kept as a stock dispersion (see Supporting Information regarding the determination of the AuNR colloid concentration).

The AuNRs synthesized with the same procedure (and by the same researcher) as reported in[39] present the following dimensions: 15±2 nm of width and 46±5 nm of length, coated by a 3 nm CTAB bilayer, determined by transmission electron microscopy (TEM) images, as shown in Figure 1, which has also a cartoon illustrating a AuNR (out-of-scale).

2.3. UV-vis spectra (absorption/solutions and extinction/colloids)

The UV-vis absorption and extinction spectra were recorded using a spectrophotometer Varian, model Cary 50, and a quartz

cuvette with 10 mm of light path (3.5 mL volume). All samples were prepared using a fixed volume of AuNRs (250 µL) and adding small aliquots from the stock solution to obtain the final concentrations of each target molecule (NiTsPc: $2.2x10^{-6}$, $6.6x10^{-6}$, and $1.6x10^{-5}$ mol L^{-1}; MB: $2.2x10^{-6}$, $2.2x10^{-5}$, and $5.5x10^{-5}$ mol L^{-1}), taking into account the dilution to a final volume of 3 mL (final volume completed with ultrapure water). Details about the sample preparation are summarized in Table 1.

2.4. Dynamic light scattering (DLS) and zeta potential

The DLS and zeta potential of AuNRs in the absence and presence of the target molecules were measured in a Malvern Zetasizer Nano ZS90 series (633 nm diode laser) at 25ºC. All samples used in this measurement were prepared following the same procedure used for extinction measurements, considering the concentration of $1.6x10^{-5}$ mol L^{-1} to NiTsPc and $2.2x10^{-5}$ to MB.

2.5. Raman, SERS, SERRS, and SEF spectra

Raman, SERS, SERRS, and SEF analysis were recorded using a micro-Raman Renishaw spectrograph, model in Via, equipped with a Leica microscope, 50x objective lens (NA 0.5). The spectra were carried out using the laser lines at 633 nm (grating of 1800 l/mm) and 785 nm (grating of 1200 l/mm), 10 s acquisition time, and one accumulation/scan. The Raman spectra of the powder target molecules were acquired using the material placed onto a microscope glass slide, while the Raman spectra of the target molecules solution at $1.0x10^{-2}$ mol L^{-1} (in water) were recorded using plastic support with a maximum volume of 400 µL, and the laser focus adjusted at the air/solution interface. SERS, SERRS, and SEF spectra from solutions diluted in the AuNR colloid were also carried out using plastic support with the laser being focused at the air/colloid interface. The SERS, SERRS, and SEF measurements were performed for both lasers using the colloid (AuNRs+target molecules) prepared as summarized in Table 1 (same condition for the extinction measurements). However, in the case of MB at 633 nm, the laser power used to record the SEF signal was 100 times greater than for fluorescence measurements.

3. Results and Discussion

3.1. Target molecules and AuNR colloid UV-vis spectra

The extinction spectrum in Figure 2 shows the AuNRs have two characteristic bands with maxima at 516 and 846 nm,

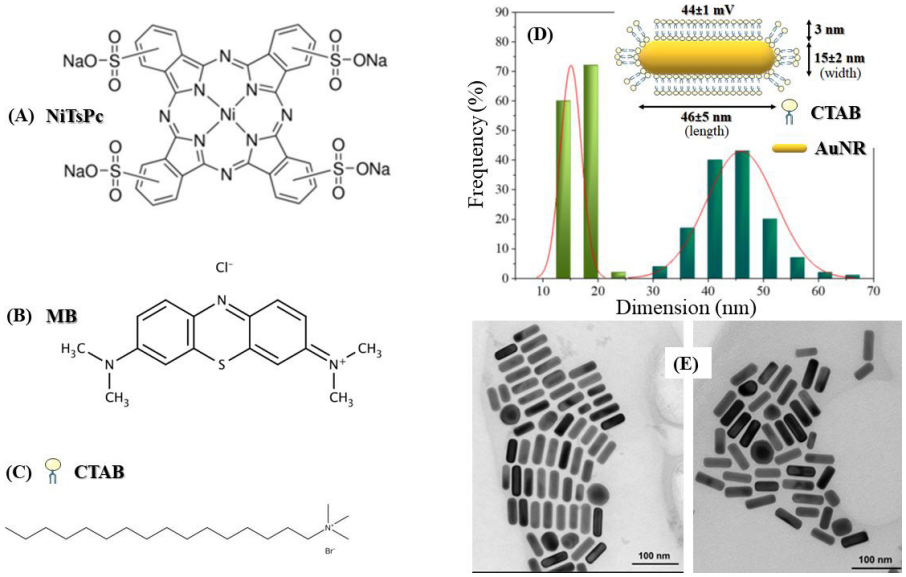

Figure 1. Molecular structures of (A) nickel(II) tetrasulfonated phthalocyanine (NiTsPc), (B) methylene blue (MB), (C) hexadecyltrimethylammonium bromide (CTAB). (D) AuNR dimension (length and width) distribution obtained from € transmission electron microscopy images (250 AuNRs were counted). Inset in (D): out-of-scale illustration of a AuNR coated with CTAB bilayer (zeta potential of 44 ±1 mV).

Table 1. preparation of the colloids (AuNRs+target molecules) used in the UV-vis extinction, DLS, zeta potential, SERS, SERRS, and SEF (before SERRS analytical application) measurements.

Sample	NiTsPc			MB		
	Stock (mol L^{-1})	*Volume added (µL)*	*Concentration (mol L^{-1})*	*Stock (mol L^{-1})*	*Volume added (µL)*	*Concentration (mol L^{-1})*
1	$3.3x10^{-4}$	20	$2.2x10^{-6}$	$3.3x10^{-4}$	20	$2.2x10^{-6}$
2	$1.0x10^{-3}$	20	$6.6x10^{-6}$	$3.3x10^{-3}$	20	$2.2x10^{-5}$
3	$1.0x10^{-3}$	50	$1.6x10^{-5}$	$3.3x10^{-3}$	50	$5.5x10^{-5}$

Final volume (cuvette) = 3 mL, volume of AuNRs = 250 µL

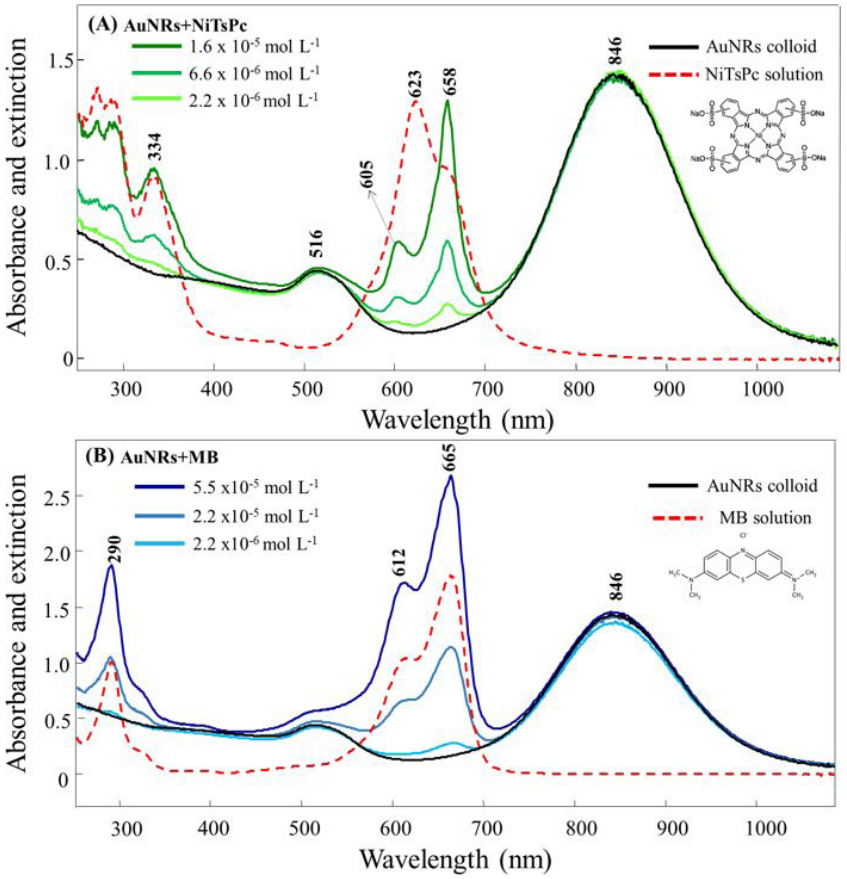

Figure 2. Extinction spectra of AuNR colloid in the absence and presence of (A) NiTsPc ($2.2x10^{-6}$, $6.6x10^{-6}$, and $1.6x10^{-5}$ mol L^{-1}) and (B) MB ($2.2x10^{-6}$, $2.2x10^{-5}$, and $5.5x10^{-5}$ mol L^{-1}). Absorption spectra of both NiTsPc ($3.3x10^{-5}$ mol L^{-1}) and MB ($3.3x10^{-5}$ mol L^{-1}) aqueous solutions are also shown. Insets: molecular structures of (A) NiTsPc and (B) MB.

which are ascribed to transverse and longitudinal plasmon bands, respectively[40]. Besides, the AuNRs, since they are coated with the CTAB bilayer, showed a positive charge surface (zeta potential: 44 ±1 mV), which can influence the adsorption of target molecules.

The UV-vis absorption spectrum of the NiTsPc shows the B-band and Q-band characteristics of metallophthalocyanines (Figure 2A), assigned to π-π* transitions. The B-band at lower wavelength is assigned to π-π* transitions from b_{1u} to e_g* (at 290 nm) and a_{2u} to e_g* orbital (334 nm), while the Q-band is ascribed to electrons transference between the a_{1u} to e_g* orbitals (HOMO-LUMO transitions)[41-43]. Besides, the Q-band can also involve the n-π* transitions[41,44], being sensible to aggregation[45].

Indeed, the Q-band shows two absorption bands with maxima at 623 and 658 nm, which correspond to the presence of aggregates and monomers, respectively[46]. In general, the metallophthalocyanines show an increase in aggregation with increasing the concentration in aqueous solutions[43,47]. However, the spectrum of NiTsPc aqueous solution diluted in AuNR colloid presents a decrease of the intensity of the band at 623 nm (aggregates) and an increase of the band at 658 nm (monomer). Since NiTsPc has negative charge SO_3^- groups, when in the presence of AuNRs, which have positive charge surface due to CTAB bilayer (quaternary ammonium salt N^+ present in the CTAB stabilized structure), the decrease observed in the NiTsPc aggregation can be ascribed to the weakening of the π-π interactions between NiTsPc molecules due to electrostatic interactions between NiTsPc (SO_3^-) and AuNRs (N^+ from CTAB bilayer). The decrease of aggregation in metallophthalocyanines was also observed by Thandekile Mthethwa et al.[46] for ZnTTAPc (thiamine substituted zinc phthalocyanine) in AuNRs at different ratios, followed by an increase in the fluorescence quantum yield due to interaction between ZnTTAPc and AuNRs; however, none explanation was given about this interaction[46].

The zeta potential at 44 ± 1 mV for neat AuNR colloid decreases to 25 ± 6 mV for AuNRs+NiTsPc ($1.6x10^{-5}$ mol L^{-1}), indicating that the negative charge of NiTsPc might neutralize part of the positive charge of the AuNRs, which is consistent with the electrostatic interaction binding NiTsPc on AuNRs, as proposed via UV-Vis data. Interesting to note is that this interaction does not promote AuNR aggregation (which could be induced by the decrease of their surface charge), as indicated by the UV-Vis extinction spectra (Figure 2A – no changes either in the band maxima or in the band width). Thus, in conclusion, the prevalence of NiTsPc aggregates in relation to monomers in aqueous solution is inverted in AuNR colloid in a way that NiTsPc adsorption may occur preferentially as monomer around the positive CTAB bilayer, and driven by electrostatic attraction (SO_3^---N^+) with no effect on the LSPR of the AuNRs.

On the other hand, unlike NiTsPc, in the UV-vis absorption spectrum of MB, the band with maxima at 612 (H-dimer – aggregates face-to-face) and 665 nm (monomers), both ascribed to π-π* transitions[48], was not affected by the AuNR colloid. The positive charge of both MB and AuNR surfaces might keep these two species far enough, minimizing changes in their aggregation levels, as indicated by none UV-Vis spectral changes. This lack of attractive interaction is also consistent with the zeta potential measured for both AuNRs (44±1 mV) and AuNRs+MB (49±3 mV at $5.5x10^{-5}$ mol L^{-1}). Thus, in conclusion, in AuNR colloid the MB may be arranged preferentially as monomers (as in aqueous solution) surrounding the positive CTAB bilayer driven by electrostatic repulsion with no effect on the LSPR of the AuNRs.

Complementary, it was observed that the increase of NiTsPc (from $2.2x10^{-6}$ to $1.6x10^{-5}$ mol L^{-1}) and MB (from $2.2x10^{-6}$ to $5.5x10^{-5}$ mol L^{-1}) concentrations in AuNR colloid changes neither the aggregate/monomer ratio for both NiTsPc and MB nor the AuNR aggregation level, as also shown by the UV-vis extinction spectra in Figure 2.

3.2. AuNR colloid dynamic light scattering

For the DLS measurements applied to nanorods, in general, the diffusion motions of the nanorods in the colloid play an important role in the intensity of the observed peaks[49,50]. The DLS does not give direct information about the dimension of the nanorods, however, it provides information about modifications around nanorod surface and medium[51]. In general, peaks with lower intensity are ascribed to rotational diffusion motion and peaks with higher intensity to longitudinal diffusion motion[49]. Based on these statements, we can observe that both NiTsPc and MB target molecules do not promote significant changes in the rotational diffusion of the AuNRs, however, the MB induces an interference on the translational diffusion (Figure 3). Because the intensity of the rotational motion peak can be related to the AuNR aggregation[50], the absence of changes in this peak suggests that the NiTsPc and MB target molecules do not induce AuNR random aggregation, which is in agreement with the extinction results. Complementary, Roejarek Kanjanawarut et al.[52] reported that DLS measurements can provide information about minor degree of AuNR assembly aggregation than UV-vis spectroscopy. Thus, the slight variation on the translational motion peak that we have observed for AuNRs suggests MB may promote some end-to-end AuNR aggregation[51,52], however not enough to change the LSPR of the AuNRs observed in the UV-vis extinction spectra (Figure 2). The end-to-end aggregation of AuNRs could be ascribed to interactions of MB (positively charge) with the tips (transverse) of the AuNR surfaces, which are less CTAB coated[52].

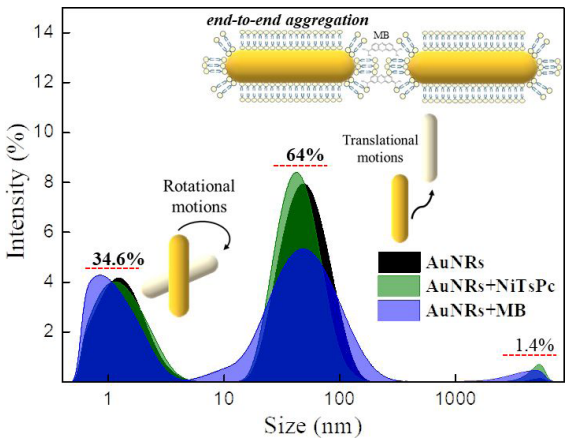

Figure 3. Dynamic light scattering (expressed as the percentage of the total scattered light intensity) of AuNR colloid in the absence and presence of NiTsPc ($1.6x10^{-5}$ mol L^{-1}) and MB ($2.2x10^{-5}$ mol L^{-1}). Inset: illustration of rotational and translational diffusion motions of nanorods in the colloid and the end-to-end aggregation in presence of MB.

3.3. SERS, SERRS, and SEF spectra

It is important to note that the Raman spectra obtained with the 633 nm are in resonance with the electronic absorption band of both NiTsPc and MB target molecules (see UV-vis absorption spectra in Figure 2), leading to RRS when in the absence of AuNRs or SERRS when in the presence of AuNRs. This double resonant effect in the case of SERRS can enhance the Raman leading to the level of single-molecule detection[12]. On the other hand, fluorescence can be achieved when working with RRS, hidden the Raman effect. In the case of the 785 nm laser line, because it is out-of-resonance with the electronic absorption of both NiTsPc and MB target molecules, the conventional Raman or SERS are achieved.

NiTsPc SERRS: the SERRS spectra of NiTsPc at $1.6x10^{-5}$ mol L^{-1} recorded in AuNR colloid (Figure 4A) with laser line at 633 nm showed the main bands at 752 (Pc ring breathing), 1188 (SO_3^- stretching), 1338 (pyrrole stretching), and 1531 cm^{-1} (isoindol stretching), which are similar in wavenumber (band center) to those observed for both powder and solution of NiTsPc (Table S1)[53-55]. These bands observed in the SERRS spectra are ascribed to in-plane vibrations, which based on SERS surface selection rules (electric field perpendicularly oriented at the metallic surface)[2,56] suggest that NiTsPc molecules are perpendicularly oriented onto the AuNR surface (preferentially).

The similarity between both RRS and SERRS spectra in terms of wavenumber band centers indicates the NiTsPc is physisorbed onto AuNRs (physical interactions), which is consistent with the previous discussion, especially because the presence of CTAB bilayer coating the Au surface, leading to the electrostatic interactions between quaternary ammonium N^+ (CTAB) and SO_3^- (NiTsPc) groups.

Besides, in our case, as a first approximation, the EF could be estimated considering SERRS/RRS intensity ratio for the integrated band at 752 cm^{-1} (I_{SERRS}/I_{RRS}), both recorded under the same experimental spectrograph setup, normalized by their concentrations ([SERRS] and [RRS]) as following, leading to an EF of ca. $2x10^2$:

$$EF \sim \frac{\frac{I_{SERRS}}{[SERRS]}}{\frac{I_{RRS}}{[RRS]}} = \frac{I_{SERRS}}{I_{RRS}} x \frac{[RRS]}{[SERRS]} = \frac{9012}{28425} x \frac{1x10^{-2}}{1.6x10^{-5}} = 198$$

This EF ~$2x10^2$ might be underestimated because the number of NiTsPc molecules in solution for Raman measurements is higher than those in SERRS measurements, once in the

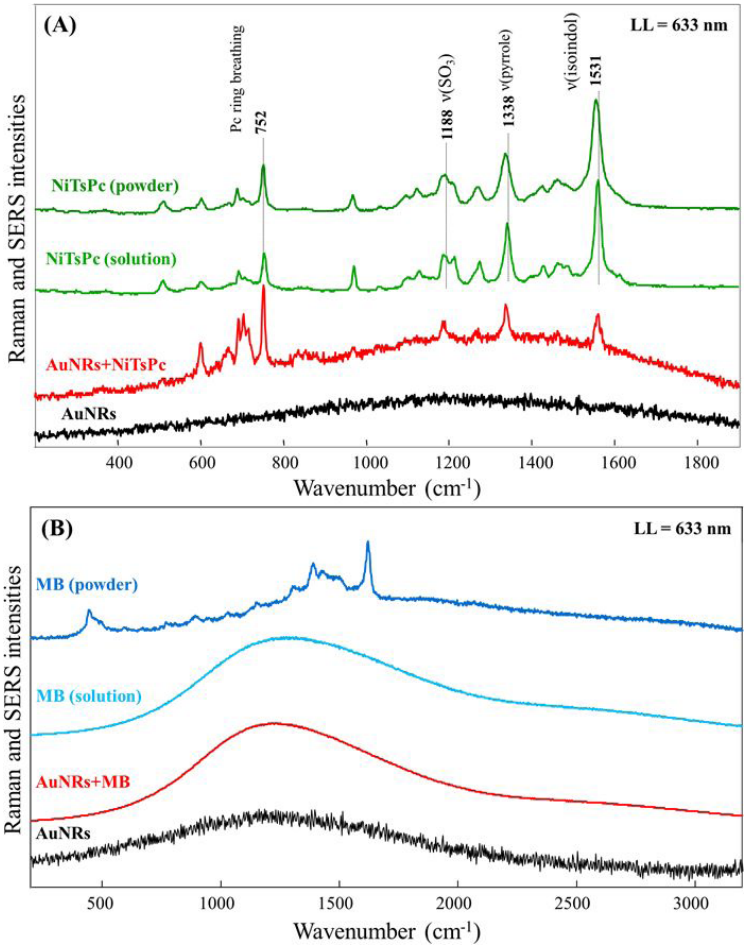

Figure 4. (A) SERRS spectrum of NiTsPc ($1.6x10^{-5}$ mol L^{-1}) and RRS spectra of NiTsPc powder and in aqueous solutions ($1.0x10^{-2}$ mol L^{-1}). (B) SEF spectrum of MB ($5.5x10^{-5}$ mol L^{-1}) using AuNR colloid, the fluorescence spectrum of MB in aqueous solutions ($1.0x10^{-2}$ mol L^{-1}), and RRS spectrum of MB powder. The Raman spectrum of neat AuNR colloid is also shown. Laser line at 633 nm.

same scattering volume, for the SERRS measurements the volume is also occupied by AuNRs (decreasing the number of NiTsPc molecules within the same scattering volume). Therefore, because SERRS is a surface effect, a more precise EF value would be find taking into account the number of NiTsPc molecules adsorbed onto the AuNR surface. In this case, considering both the NiTsPc adsorption is governed by the number of CTAB molecules coating the AuNR surface and the number of AuNRs in the scattering volume, an EF around 10^5 was found as following (the detailed calculation is given in the Supporting Information):

$$EF = \frac{\frac{I_{SERRS}}{N_{SERRS}}}{\frac{I_{RRS}}{N_{RRS}}} = \frac{I_{SERRS}}{I_{RRS}} \times \frac{N_{RRS}}{N_{SERRS}} = \frac{9012}{28425} \times \frac{1.81x10^{19}}{4.83x10^{13}} = 1.2x10^5$$

N_{RRS} is the number of NiTsPc molecules in a certain volume (aqueous solution) and N_{SERRS} is the number of NiTsPc molecules coating the AuNRs in the same certain volume (colloid). The signal enhancement is basically induced by the enhancement of the electromagnetic field surrounding the AuNRs (electromagnetic effect - physisorption) instead of any chemisorption that would lead to a complex NiTsPc-Au (chemical effect).

Because SERS (or SERRS) is a distance-dependent effect, the closer the target molecule to the metal surface, the higher the EF of the Raman signal, where the contact between both is the optimum condition[2,57]. Therefore, in our case, despite the CTAB bilayer (~3 nm) surrounding the Au surface, a fair EF due to AuNRs is still observed. Kovacs et al.[57] described a distance dependence on the EF for tert-butylphthalocyanine ($(t\text{-}Bu)_4H_2Pc$ - metal free) onto Ag island surfaces. The maximum EF around 10^2 was observed for a distance of 2-3 nm between the target molecule and the Ag surface[57]. An EF around 10^2 was also observed for copper phthalocyanine film (4 nm) deposited onto Ag substrate ("nearly spherical particles with diameters of ≈ 200 nm"), as described by Horimoto et al.[58]. Losytskyy et al.[59] described that a concentration of $5.0x10^{-7}$ mol L^{-1} of hafnium phthalocyanine dichloride dried with AgNP in a glass substrate provides an EF of $4.5x10^4$ for the band at 759 cm^{-1}, which as applied for detection of fibrillar insulin (amyloidogenic protein insulin). Aroca et al.[60] described that lutetium and ytterbium bis-phthalocyanine film with 10 nm of thickness deposited onto Ag islands (15 nm) showed an EF of 500 for SERRS

measurements (laser line 641 nm). Thus, the EF we have observed for NiTsPc onto AuNR surfaces is similar or higher to those observed for metallophthalocyanine films applied in SERS (or SERRS) measurements. However, the differences in the interaction between the target molecule (film and aqueous medium) and the SERS substrate (solid and colloid; Au and Ag) must be considered.

In general, the MTsPc with different metal centers shows similar Raman spectra and poor SERS signal when using Ag or Au surfaces (sols)[59,61,62]. However, modification of the colloid with positive surfactants can help the enhancement of Raman signal of MTsPc[61]. Jong-Seo Ha et al.[61] reported the NiTsPc SERS signal using Ag sol with the addition of surfactants as CTAC (cetyltrimethylammonium chloride) and CTAB. The authors ascribed this effect to the interaction of the ammonium group of the surfactant and the anionic SO_3^- group of the NiTsPc molecules, which allow the NiTsPc adsorption onto the Ag surface[61], in agreement with we have observed here. Lokesh et al.[37] also observed that the nitrogen atom of the amine groups on the periphery structure of cobalt tetraamino phthalocyanine (CoPcTA) can interact with Au and Ag nanoparticle surfaces, showing an EF of 10 in comparison with the CoPcTA solution (10^{-6} mol L^{-1}). These works showed that both target molecule and nanoparticle charges play an important role in the efficiency of the EF SERS signal. Thus, for target molecules with negative charge, the CTAB bilayer (positive layer) plays a key role to obtain the SERS (or SERRS) signal.

MB SEF: in the case of MB at $5.5x10^{-5}$ mol L^{-1} in AuNRs excited with the 633 nm laser line (Figure 4B), only an enhancement of MB fluorescence was observed (SEF). Using the same "first approximation" applied to estimate the SERRS EF for NiTsPc, we have compared the SEF spectrum with the fluorescence (F) one for MB in aqueous solution, both recorded under the same spectrograph setup (except laser power), and normalized by their concentrations. Then, the EF was estimated by the ratio of their maximum intensities (peak intensity = band height),

$$EF \sim \frac{\frac{I_{SEF}}{[SEF]}}{\frac{I_F}{[F]}} = \frac{I_{SEF}}{I_F} x \frac{[F]}{[SEF]} = \frac{127819}{24838} x \frac{1x10^{-2}}{5.5x10^{-5}} = 935 ,$$

and corrected considering the laser power used to record the SEF signal was 100 times greater, leading to an EF of ca. 10^1.

Using the number of MB molecules (N) in aqueous solution (N_F) and those adsorbed onto the AuNRs (N_{SEF}), both for a certain volume, as described for SERRS/RRS, an EF of ca. 10^4 would be found, where I_{SEF} or I_F = peak intensity = band height (detailed calculation in the Supporting Information):

$$EF = \frac{\frac{I_{SEF}}{N_{SEF}}}{\frac{I_F}{N_F}} = \frac{I_{SEF}}{I_F} \times \frac{N_F}{N_{SEF}} = \frac{127819}{24838} \times \frac{1.81x10^{19}}{4.83x10^{13}} = 193x10^4 .$$

Considering the laser power used to record the SEF signal was 100 times greater, the EF is $1.93x10^4 \sim 10^4$. However, this value is pretty high for SEF and seems to be unreal, consequence of the assumption that we would have one molecule of MB for one molecule of CTAB (1 MB: 1 CTAB) adsorbing onto the AuNR surface, as we considered for NiTsPc. In the case of MB, this assumption should not be applied since MB is cationic as well as CTAB, which would lead to a repuslsion interaction. Based on this observation, the EF of ca. 10^1 would be more realistic for SEF in this case.

Usually, when the emitter group of the fluorescent molecule is in contact with the metal surface, a quenching of the fluorescence is observed, existing an optimum distance for which the enhancement of the fluorescence is optimized[2,63]. Indeed, the increase of the distance between MB and nanoparticle surface leads to a decrease in the SERS signal[64] and provides an enhancement of the fluorescence[65]. In the case of MB onto AuNRs, de CTAB bilayer (thickness ~3 nm) is responsible for avoiding this contact and, as a consequence, avoinding the fluorescence quenching. Indeed, an EF of ca. 10^1 is expected according to Weitz et al.[66] for molecules adsorbed onto rough Ag surfaces: in average, SERS: 10^5; SERRS: 10^3; SEF: 10^{-1} – 10^1, depending on the quantum yield of the fluorescent molecule. An EF of 1000 ±100 for MB in "spermine induced co-aggregation of dye-labeled DNA and Ag nanoparticles" was described by Gill et al.[67]. On the other hand, the quenching of the MB was observed by Naujok et al.[68] when MB is adsorbed directly onto Au surface.

NiTsPc and MB SERS: the importance of the resonant effect to obtain RRS or SERRS for metallophthalocyanine in general, and NiTsPc in this case, is highlighted when the experiment is carried out using the laser line at 785 nm (Figure 5), which is out of resonance with NiTsPc electronic absorption. The NiTsPc Raman signal presents fewer bands than RRS and, in the case of SERS, the CTAB bilayer between NiTsPc and Au surface is already enough to practically vanish the SERS effect. The importance of the resonant effect to obtain SERS or SERRS signal from copper phthalocyanine (CoPc) on Au substrates was reported by Sheremet et al.[69], being observed an EF of 85 for SERRS (laser line 632.3 nm) and 19 for SERS (514.5 nm). The resonance with the nanoparticle can also be an important factor to be considered in the low or vanish SERS effect. For instance,

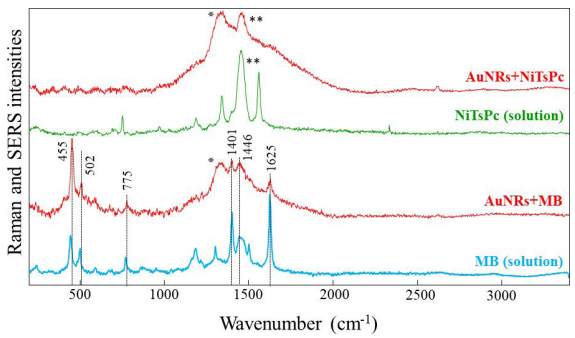

Figure 5. SERS spectra of NiTsPc ($1.6x10^{-5}$ mol L^{-1}) and MB ($5.5x10^{-5}$ mol L^{-1}) using AuNRs. Raman spectra of both NiTsPc and MB in an aqueous solution ($1.0x10^{-2}$ mol L^{-1}) are also shown. Spectra applying the baseline correction. Laser line at 785 nm. *Background signal (low intensities) from laser line at 785 nm, which can be observed only when the target molecule (or analyte) shows a poor signal. **Band ascribed to the plastic support.

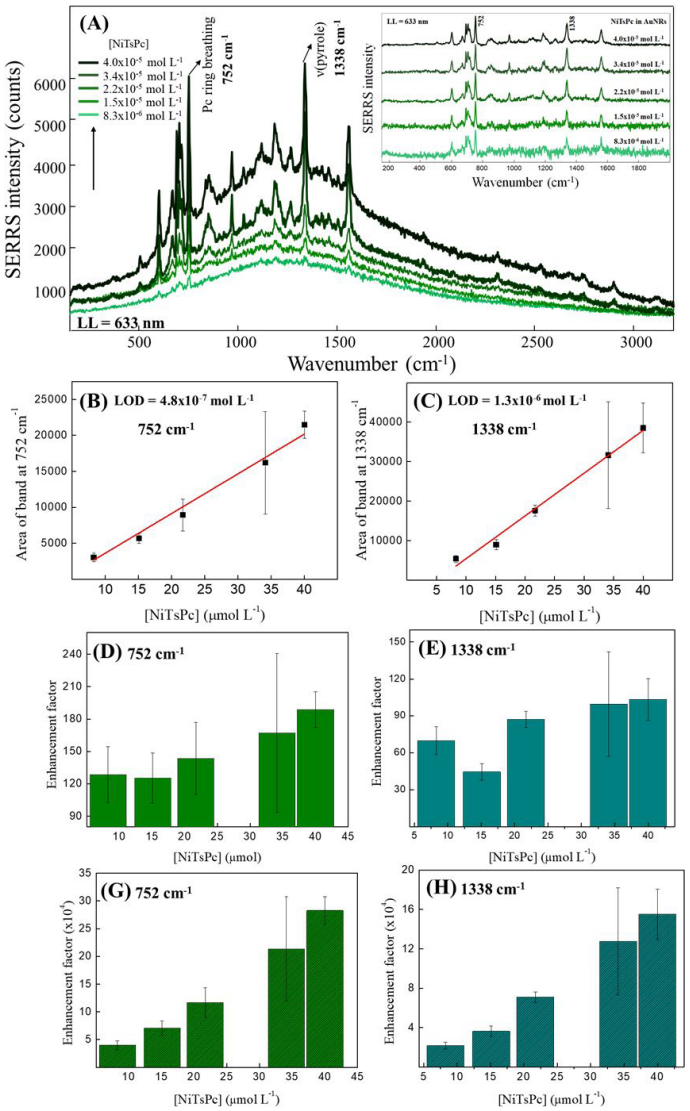

Figure 6. SERRS spectra of NiTsPc at different concentrations in AuNR colloid. (A) Increasing the SERRS intensity with increasing the NiTsPc from $8.3x10^{-6}$ to $4.0x10^{-5}$ mol L^{-1}. Inset: SERRS spectra of NiTsPc from (A) applying the baseline correction. Variation of the SERRS intensity at (B) 752 and (C) 1338 cm^{-1} with increasing the NiTsPc concentration. Enhancement factor determined using the normalization from molar concentration ratio for the bands at (D) 752 and (E) 1338 cm^{-1}. Enhancement factor determined using the normalization by the number of NiTsPc molecules coating the AuNR surface for the bands at (F) 752 and (G) 1338 cm^{-1}. The SERRS spectra, variation of SERRS intensity, and EF observed for NiTsPc from $8.3x10^{-6}$ to $8.2x10^{-5}$ mol L^{-1} are shown in Figure S1 (Supporting Information).

the CoPc deposited on Au nanoantennas[70] led to an EF of 9, while in Au nanocluster[71] the EF was $2x10^4$ (both results using the 632.8 nm laser line in resonance with the CoPc molecule). The differences are ascribed to the resonance of the laser with both nanocluster and CoPc, which provides a higher EF. In the case of Au nanoantennas, the laser line is in resonance only with the CoPc.

On the other hand, using the laser line at 785 nm, it was possible to obtain the MB SERS spectrum (Figure 5), whose main bands are found at 455 (skeletal deformation of C-N-C), 502 (skeletal deformation of C-N-C), 775 (in-plane bending of C-H), 1401 (symmetrical stretching of C-N), 1446 (asymmetrical stretching of C-N), and 1625 cm^{-1} (ring stretching of C-C). These MB SERS bands are similar to those observed for Raman spectrum of MB in solution (Table S2)[6,35,72], which indicates the MB is also physisorbed onto the AuNRs, as previously discussed for NiTsPc. A similar effect was observed by Fales et al.[65] using the MB silica-coated Au nanostars and the laser line at 785 nm, for which the SERS spectrum of MB was observed, even without direct contact of MB with the Au surface.

3.4. The concentration effect of the NiTsPc on SERRS signal (quantitative analysis)

The effect of NiTsPc concentration on SERRS signal (Figure 6) was carried out using a fixed AuNR volume (400 μL) and the multiple standard method (see details in Supporting Information). The analysis was performed considering the integrated area of the SERRS bands at

752 (Pc ring breathing) and at 1338 cm^{-1} (pyrrole stretching). Both bands showed a linear increase of the SERRS intensity (integrated area) vs NiTsPc concentration in AuNRs from $8.3x10^{-6}$ to $4.0x10^{-5}$ mol L^{-1}, as shown in Figures 6B (752 cm^{-1}) and 6C (1338 cm^{-1}). Considering this linear range, the limit of detection (LOD) was calculated from equation *3xSD/S* [73], where *SD* is the standard deviation of the "Raman signal" of the AuNR colloid in the absence of the NiTsPc (blank sample) and *S* is the slope of the linear equation (sensitivity) (all details are described in the Supporting Information). The LOD was found to be $4.8x10^{-7}$ using the band at 752 cm^{-1} and $1.3x10^{-6}$ mol L^{-1} using the band at 1338 cm^{-1}. The inset in Figure 6A shows the SERRS spectral profiles are the same, independent of the NiTsPc concentration, which indicates the adsorption mechanism of NiTsPc onto AuNRs is the same (for this concentration range), as previously discussed (Figure 4A). Otherwise, considering the SERS surface selection rules, changes in relative intensities should be observed.

Complementary, Figures 6D-6G show the EF for SERRS/RRS against NiTsPc concentration using both 752 and 1338 cm^{-1} bands. In the case of Figures 6D and 6E, we have estimated the EF using the concentrations of the NiTsPc in the aqueous solution and in the AuNR colloid ($EF = \frac{\frac{I_{SERRS}}{[SERRS]}}{\frac{I_{RRS}}{[RRS]}}$). In the case of Figures 6F and 6G, we have estimated the EF using the number of NiTsPc in a certain volume in the aqueous solution and the number of NiTsPc coating the AuNRs in the same certain volume of the AuNR colloid ($EF = \frac{\frac{I_{SERRS}}{N_{SERRS}}}{\frac{I_{RRS}}{N_{RRS}}}$). In both cases, the I_{RRS} was used from resonance Raman spectrum of NiTsPc in aqueous solution at 10^{-2} mol L^{-1}.

It is interesting to note that the EF is consistently higher for the band at 752 cm^{-1} (comparing the same concentrations), independent of the way how it was determined. This pattern is consistent with the electromagnetic mechanism, for which, the closer the band to the excitation laser line, the higher the EF[2,60]. Still from Figures 6D and 6E, and specially for Figures 6F and 6G, there is a tendency of the EF increases with the NiTsPc concentration within the linear range (Figures 6B and 6C). However, it is important to note that the NiTsPc concentrations used here imply that there are more molecules of NiTsPc than CTAB. Thus, after the first layer of NiTsPc surrounding the AuNRs, other layers composed by NiTsPc monomers and/or aggregates could be formed[19]. Therefore, these NiTsPc molecules adsorbing onto the first layer of NiTsPc coating the AuNRs might be also contributing to the enhancing of the Raman signal.

4. Conclusion

AuNRs coated with a positive CTAB bilayer (ca. 44 mV zeta potential) have been applied to investigate their plasmonic effect on charged molecules. The anionic NiTsPc molecules, which are preferentially arranged as aggregates in aqueous solution, are physisorbed preferentially as monomer onto AuNRs, perpendicularly oriented, and driven by electrostatic interactions between sulfonated SO_3^- (NiTsPc) and quaternary ammonium N^+ (CTAB) groups. The NiTsPc presented a maximum SERRS EF about 10^5, which shows to be dependent on both the NiTsPc concentration and the NiTsPc band considered. Besides, the AuNRs allow the analytical application of the SERRS effect for NiTsPc reaching a minimum LOD of $4.8x10^{-7}$ mol L^{-1} for the band at 752 cm^{-1} (standard addition method). In the case of the cationic MB molecules, they are preferentially arranged as monomers on both aqueous solution and AuNR colloid, being physisorbed onto the AuNRs, which allows achieving the SEF effect with an EF about 10. Basically, the surfactant bilayer surrounding the Au surface played an important role in two basic aspects: it promotes the adsorption of the anionic NiTsPc onto the AuNRs allowing the enhancement of the Raman signal and keep the MB far enough from the Au surface allowing the enhancement of the MB fluorescence signal. Therefore, the benefits of the plasmonic effect of the AuNRs coated with the positive CTAB bilayer presented here show to be a suitable approach for enhancing either the Raman or the fluorescence signals for charged target molecules, besides supporting studies designed for the application of SERRS (or SERS) as analytical tool.

5. Acknowledgments

This study was financed in part by the "Coordenação de Aperfeiçoamento de Pessoal de Nível Superior – Brasil (CAPES) – Finance Code 001" CAPES, besides CNPq, INCT/INEO, and FAPESP 2018/22214-6 (Brazilian funding agencies).

6. References

1. Aroca RF, Alvarez-Puebla RA, Pieczonka N, Sanchez-Cortez S, Garcia-Ramos JV. Surface-enhanced Raman scattering on colloidal nanostructures. Adv Colloid Interface Sci. 2005;116(1-3):45-61.
2. Aroca R. Surface-enhanced vibrational spectroscopy. Chichester, UK: John Wiley & Sons; 2006.
3. Le Ru EC, Grand J, Sow I, Somerville WRC, Etchegoin PG, Treguer-Delapierre M, et al. A scheme for detecting every single target molecule with Surface-Enhanced Raman Spectroscopy. Nano Lett. 2011;11(11):5013-9.
4. Mitsutake H, Poppi R, Breitkreitz M. Raman imaging spectroscopy: history, fundamentals and current scenario of the technique. J Braz Chem Soc. 2019;30(11):2243-58.
5. Rubira RJG, Camacho SA, Aoki PHB, Maximino MD, Alessio P, Martin CS, et al. Detection of trace levels of atrazine using surface-enhanced Raman scattering and information visualization. Colloid Polym Sci. 2014;292(11):2811-20.
6. Li C, Huang Y, Lai K, Rasco BA, Fan Y. Analysis of trace methylene blue in fish muscles using ultra-sensitive surface-enhanced Raman spectroscopy. Food Control. 2016;65:99-105.
7. Aroca RF. Plasmon enhanced spectroscopy. Phys Chem Chem Phys. 2013;15(15):5355.
8. Le Ru EC, Etchegoin PG. Principles of Surface-Enhanced Raman Spectroscopy. Amsterdam: Elsevier; 2009.
9. Otto A. The 'chemical' (electronic) contribution to surface-enhanced Raman scattering. J Raman Spectrosc. 2005;36(6-7):497-509.

10. Nie S. Probing single molecules and single nanoparticles by surface-enhanced raman scattering. Science. 1997;275(5303):1102-6.
11. Kneipp K, Wang Y, Kneipp H, Perelman LT, Itzkan I, Dasari RR, et al. Single molecule detection using Surface-Enhanced Raman Scattering (SERS). Phys Rev Lett. 1997;78(9):1667-70.
12. Constantino CJL, Lemma T, Antunes PA, Aroca R. Single-molecule detection using surface-enhanced resonance raman scattering and Langmuir-Blodgett monolayers. Anal Chem. 2001;73(15):3674-8.
13. Kim J, Sim K, Cha S, Oh J, Nam J. Single-particle analysis on plasmonic nanogap systems for quantitative SERS. J Raman Spectrosc. 2020;52:375-385.
14. Pajerski W, Ochonska D, Brzychczy-Wloch M, Indyka P, Jarosz M, Golda-Cepa M, et al. Attachment efficiency of gold nanoparticles by Gram-positive and Gram-negative bacterial strains governed by surface charges. J Nanopart Res. 2019;21(8):186.
15. Prakash J, Swart HC, Zhang G, Sun S. Emerging applications of atomic layer deposition for the rational design of novel nanostructures for surface-enhanced Raman scattering. J Mater Chem C Mater Opt Electron Devices. 2019;7(6):1447-71.
16. Li M, Zhang X. Nanostructure-based surface-enhanced raman spectroscopy techniques for pesticide and veterinary drug residues screening. bull environ contam toxicol. 2020. In press.
17. Zhang D, Liang P, Yu Z, Xia J, Ni D, Wang D, et al. Self-assembled "bridge" substance for organochlorine pesticides detection in solution based on Surface Enhanced Raman Scattering. J Hazard Mater. 2020;382:121023.
18. Hassan MM, Zareef M, Jiao T, Liu S, Xu Y, Viswadevarayalu A, et al. Signal optimized rough silver nanoparticle for rapid SERS sensing of pesticide residues in tea. Food Chem. 2021;338:127796.
19. Oliveira MJS, Rubira RJG, Furini LN, Batagin-Neto A, Constantino CJL. Detection of thiabendazole fungicide/parasiticide by SERS: quantitative analysis and adsorption mechanism. Appl Surf Sci. 2020;517:145786.
20. Dey S, Trau M, Koo KM. Surface-enhanced raman spectroscopy for cancer immunotherapy applications: opportunities, challenges, and current progress in nanomaterial strategies. Nanomaterials. 2020;10(6):1145.
21. Wang H-N, Register JK, Fales AM, Gandra N, Strobbia P, Cho EH, et al. Implantable "smart tattoo" SERS nanosensors for in vivo detection of nucleic acid biotargets in a large animal model. In: Vo-Dinh T, Ho H-PA, Ray K, editors. Plasmonics in Biology and Medicine XVI; 2019; San Francisco, CA. Proceedings. Bellingham, WA: SPIE; 2019. p. 54.
22. Shim K-D, Jang E-S. SERS signal enhancement of methylene blue-embedded agglomerated gold nanorod@SiO_2 core@shell composites. Bull Korean Chem Soc. 2018;39(8):936-40.http://dx.doi.org/10.1002/bkcs.11528.
23. Du Z, Qi Y, He J, Zhong D, Zhou M. Recent advances in applications of nanoparticles in SERS in vivo imaging. Wiley Interdiscip Rev Nanomed Nanobiotechnol. 2021;13(2):e1672.
24. Ahlawat M, Sarkar A, Roy S, Jaiswal A. Gold nanorattles with intense raman in silica nanoparticles (Nano-IRIS) as multimodal system for imaging and therapy. ChemNanoMat. 2019;5(5):625-33.
25. Darienzo RE, Chen O, Sullivan M, Mironava T, Tannenbaum R. Au nanoparticles for SERS: temperature-controlled nanoparticle morphologies and their Raman enhancing properties. Mater Chem Phys. 2020;240:122143.
26. Alwan AM, Mohammed MS, Shehab RM. Modified laser-etched silicon covered with bimetallic Ag-Au Alloy nanoparticles for high-performance SERS: laser wavelength dependence. Indian J Phys. 2020. In press.
27. Wang Y, Shang B, Liu M, Shi F, Peng B, Deng Z. Hollow polydopamine colloidal composite particles: structure tuning, functionalization and applications. J Colloid Interface Sci. 2018;513:43-52.
28. Rubira RJG, Camacho SA, Martin CS, Mejía-Salazar JR, Reyes Gómez F, da Silva RR, et al. designing silver nanoparticles for detecting levodopa (3,4-Dihydroxyphenylalanine, L-Dopa) using Surface-Enhanced Raman Scattering (SERS). Sensors. 2019;20(1):15.
29. Wei H, Vikesland PJ. pH-triggered molecular alignment for reproducible SERS detection via an AuNP/nanocellulose platform. Sci Rep. 2015;5(1):18131.
30. Li J-J, An H-Q, Zhu J, Zhao J-W. Improve the surface enhanced Raman scattering of gold nanorods decorated graphene oxide: the effect of CTAB on the electronic transition. Appl Surf Sci. 2015;347:856-60.
31. Garcia-Leis A, Torreggiani A, Garcia-Ramos JV, Sanchez-Cortes S. Hollow Au/Ag nanostars displaying broad plasmonic resonance and high surface-enhanced Raman sensitivity. Nanoscale. 2015;7(32):13629-37.
32. Furini LN, Martin CS, Camacho SA, Rubira RJG, Fernandes JD, Silva EA, et al. Electrochemical properties of nickel phthalocyanine: the effect of thin film morphology tuned by deposition techniques. Thin Solid Films. 2020;699:137897.
33. Rubira RJG, Aoki PHB, Constantino CJL, Alessio P. Supramolecular architectures of iron phthalocyanine Langmuir-Blodgett films: the role played by the solution solvents. Appl Surf Sci. 2017;416:482-91.
34. Zoleo A, Rossi C, Poggi G, Rossi M, Meneghetti M, Baglioni P. Spotting aged dyes on paper with SERS. Phys Chem Chem Phys. 2020;22(41):24070-6.
35. Xu T, Wang X, Huang Y, Lai K, Fan Y. Rapid detection of trace methylene blue and malachite green in four fish tissues by ultra-sensitive surface-enhanced Raman spectroscopy coated with gold nanorods. Food Control. 2019;106:106720.
36. Chen J, Sun K, Zhang Y, Wu D, Jin Z, Xie F, et al. Plasmonic MoO_2 nanospheres assembled on graphene oxide for highly sensitive SERS detection of organic pollutants. Anal Bioanal Chem. 2019;411(13):2781-91.
37. Lokesh KS, Narayanan V, Sampath S. Phthalocyanine macrocycle as stabilizer for gold and silver nanoparticles. Mikrochim Acta. 2009;167(1-2):97-102.
38. Xu D, Mao J, He Y, Yeung ES. Size-tunable synthesis of high-quality gold nanorods under basic conditions by using H_2O_2 as the reducing agent. J Mater Chem C Mater Opt Electron Devices. 2014;2(25):4989.
39. Barros A, Shimizu FM, de Oliveira CS, Sigoli FA, Santos DP, Mazali IO. Dynamic behavior of surface-enhanced raman spectra for rhodamine 6G interacting with gold nanorods: implication for analyses under wet versus dry conditions. ACS Applied Nano Materials. 2020;3(8):8138-47.
40. Cao J, Sun T, Grattan KTV. Gold nanorod-based localized surface plasmon resonance biosensors: a review. Sens Actuators B Chem. 2014;195:332-51.
41. Mack J, Stillman MJ. Transition Assignments in the Ultraviolet-visible absorption and magnetic circular dichroism spectra of phthalocyanines. Inorg Chem. 2001;40(4):812-4.
42. Gaffo L, Constantino CJL, Moreira WC, Aroca RF, Oliveira ON. Atomic force microscopy and micro-Raman imaging of mixed Langmuir-Blodgett films of ytterbium bisphthalocyanine and stearic acid. Langmuir. 2002;18(9):3561-6.
43. Wöhrle D. Phthalocyanines: properties and applications. Edited by C. C. Leznoff and A. B. P. Lever, VCH, Weinheim. Volume 1, 1989, 436 pp., ISBN 3-527-26955-X; Volume 2, 1993, 305 pp., DM 268, ISBN 3-527-89544-2. Adv Mater. 1993;5(12):942-3.
44. Zanfolim AA, Volpati D, Olivati CA, Job AE, Constantino CJL. Structural and electric-optical properties of zinc phthalocyanine evaporated thin films: temperature and thickness effects. J Phys Chem C. 2010;114(28):12290-9.

45. Vlaskin V, Dimitriev O, Kazantseva Z, Nabok A. Association of some phthalocyanines: from solutions to thin films. Thin Solid Films. 1996;286(1-2):40-4.
46. Mthethwa T, Antunes E, Nyokong T. Photophysical properties of a new water soluble tetra thiamine substituted zinc phthalocyanine conjugated to gold nanorods of different aspect ratios. Dalton Trans. 2014;43(22):8230.
47. Martin CS, Alessio P, Crespilho FN, Constantino CJL. Supramolecular arrangement of iron phthalocyanine in langmuir-schaefer and electrodeposited thin films. J Nanosci Nanotechnol. 2018;18(5):3206-17.
48. Jacobs KY, Schoonheydt RA. Spectroscopy of Methylene Blue-Smectite Suspensions. J Colloid Interface Sci. 1999;220(1):103-11.
49. Glidden M, Muschol M. Characterizing gold nanorods in solution using depolarized dynamic light scattering. J Phys Chem C. 2012;116(14):8128-37.
50. Liu H, Pierre-Pierre N, Huo Q. Dynamic light scattering for gold nanorod size characterization and study of nanorod-protein interactions. Gold Bull. 2012;45(4):187-95.
51. Pellas V, Hu D, Mazouzi Y, Mimoun Y, Blanchard J, Guibert C, et al. Gold nanorods for LSPR biosensing: synthesis, coating by silica, and bioanalytical applications. Biosensors. 2020;10(10):146.
52. Kanjanawarut R, Yuan B, XiaoDi S. UV-Vis spectroscopy and dynamic light scattering study of gold nanorods aggregation. Nucleic Acid Ther. 2013;23(4):273-80. http://dx.doi.org/10.1089/nat.2013.0421.
53. Zucolotto V, Ferreira M, Cordeiro MR, Constantino CJL, Balogh DT, Zanatta AR, et al. Unusual interactions binding iron tetrasulfonated phthalocyanine and poly(allylamine hydrochloride) in layer-by-layer films. J Phys Chem B. 2003;107(16):3733-7.
54. Gaffo L, Constantino CJL, Moreira WC, Aroca RF, Oliveira ON. Vibrational spectra and surface-enhanced resonance Raman scattering of palladium phthalocyanine evaporated films. J Raman Spectrosc. 2002;33(10):833-7.
55. Verma D, Dash R, Katti KS, Schulz DL, Caruso AN. Role of coordinated metal ions on the orientation of phthalocyanine based coatings. Spectrochim Acta A Mol Biomol Spectrosc. 2008;70(5):1180-6.
56. Figueiredo MLB, Martin CS, Furini LN, Rubira RJG, Batagin-Neto A, Alessio P, et al. Surface-enhanced Raman scattering for dopamine in Ag colloid: adsorption mechanism and detection in the presence of interfering species. Appl Surf Sci. 2020;522:146466.
57. Kovacs GJ, Loutfy RO, Vincett PS, Jennings C, Aroca R. Distance dependence of SERS enhancement factor from Langmuir-Blodgett monolayers on metal island films: evidence for the electromagnetic mechanism. Langmuir. 1986;2(6):689-94.
58. Horimoto N, Ishikawa N, Nakajima A. Preparation of a SERS substrate using vacuum-synthesized silver nanoparticles. Chem Phys Lett. 2005;413(1-3):78-83.
59. Losytskyy M, Akbay N, Chernii S, Avcı E, Chernii V, Yarmoluk S, et al. Characterization of the Interaction between phthalocyanine and amyloid fibrils by Surface-Enhanced Raman Scattering (SERS). Anal Lett. 2018;51(1-2):221-8.
60. Aroca R, Clavijo RE, Jennings CA, Kovacs GJ, Duff JM, Loutfy RO. Vibrational spectra of lutetium and ytterbium bis-phthalocyanine in thin solid films and SER€S on silver island films. Spectrochim Acta A. 1989;45(9):957-62.
61. Ha J-S, Yoon M, Lee M, Jang D-J, Kim D. Surfactant-aided surface enhanced Raman scattering of Ni(II) tetrasulphonate phthalocyanine in silver sol. J Raman Spectrosc. 1991;22(10):597-600.
62. Lee PC, Meisel D. Adsorption and surface-enhanced Raman of dyes on silver and gold sols. J Phys Chem. 1982;86(17):3391-5.
63. Antunes PA, Constantino CJL, Aroca RF, Duff J. Langmuir and Langmuir-Blodgett films of perylene tetracarboxylic derivatives with varying alkyl chain length: film packing and surface-enhanced fluorescence studies. Langmuir. 2001;17(10):2958-64.
64. Aoki PHB, Alessio P, De Saja JÁ, Constantino CJL. Incorporation of Ag nanoparticles into membrane mimetic systems composed by phospholipid layer-by-layer (LbL) films to achieve surface-enhanced Raman scattering as a tool in drug interaction studies. J Raman Spectrosc. 2010;41(1):40-8.
65. Fales AM, Yuan H, Vo-Dinh T. Silica-coated gold nanostars for combined Surface-Enhanced Raman Scattering (SERS) detection and singlet-oxygen generation: a potential nanoplatform for theranostics. Langmuir. 2011;27(19):12186-90.
66. Weitz DA, Garoff S, Gersten JI, Nitzan A. The enhancement of Raman scattering, resonance Raman scattering, and fluorescence from molecules adsorbed on a rough silver surface. J Chem Phys. 1983;78(9):5324-38.
67. Gill R, Tian L, van Amerongen H, Subramaniam V. Emission enhancement and lifetime modification of phosphorescence on silver nanoparticle aggregates. Phys Chem Chem Phys. 2013;15(38):15734..
68. Naujok RR, Duevel RV, Corn RM. Fluorescence and Fourier Transform surface-enhanced Raman scattering measurements of methylene blue adsorbed onto a sulfur-modified gold electrode. Langmuir. 1993;9(7):1771-4.
69. Sheremet E, Rodriguez RD, Zahn DRT, Milekhin AG, Rodyakina EE, Latyshev AV. Surface-enhanced Raman scattering and gap-mode tip-enhanced Raman scattering investigations of phthalocyanine molecules on gold nanostructured substrates. J Vac Sci Technol B. 2014;32(4):04E110.
70. Milekhin AG, Cherkasova O, Kuznetsov SA, Milekhin IA, Rodyakina EE, Latyshev AV, et al. Nanoantenna-assisted plasmonic enhancement of IR absorption of vibrational modes of organic molecules. Beilstein J Nanotechnol. 2017;8:975-81.
71. Milekhin AG, Yeryukov NA, Sveshnikova LL, Duda TA, Rodyakina EE, Sheremet ES, et al. Surface enhanced Raman scattering by organic and inorganic semiconductors formed on laterally ordered arrays of Au nanoclusters. Thin Solid Films. 2013;543:35-40.
72. Aoki PHB, Volpati D, Caetano W, Constantino CJL. Study of the interaction between cardiolipin bilayers and methylene blue in polymer-based Layer-by-Layer and Langmuir films applied as membrane mimetic systems. Vib Spectrosc. 2010;54(2):93-102.
73. Shrivastava A, Gupta V. Methods for the determination of limit of detection and limit of quantitation of the analytical methods. Chronicles of Young Scientists. 2011;2(1):21.

Supplementary material

The following online material is available for this article: Supplementary Material - Enhancement Factor (EF).